Applied Energy 314 (2022) 118887

Contents lists available at ScienceDirect

Applied Energy

journal homepage: www.elsevier.com/locate/apenergy

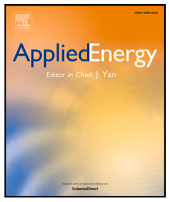

A multi-objective framework for distributed energy resources planning and storage management

Bahman Ahmadi [a], Oguzhan Ceylan [b], Aydogan Ozdemir [c,*], Mahmoud Fotuhi-Firuzabad [d]

[a] Department of Electrical Engineering, Mathematics and Computer Science, University of Twente, Enschede, Netherlands
[b] Department of Electrical and Electronics Engineering, Marmara University, Istanbul, Turkey
[c] Department of Electrical Engineering, Istanbul Technical University, Istanbul, Turkey
[d] Electrical Engineering Department, Sharif University of Technology, Tehran, Iran

ARTICLE INFO

Keywords:
Distributed energy sources
Heuristic algorithms
Multi-objective optimization
Power system planning
Reliability
Network losses

ABSTRACT

The use of energy storage systems (ESS) and distributed generators (DGs) to improve reliability is one of the solutions that has received much attention from researchers today. In this study, we utilize a multi-objective optimization method for optimal planning of distributed generators in electric distribution networks from the perspective of multi-objective optimization. The objective is to improve the reliability of the network while reducing the annual cost and network losses. A modified version of the multi-objective sine–cosine algorithm is used to determine the optimal size, location, and type of DGs and the optimal capacity, location, and operation strategy of the ESS. Three case studies of IEEE 33-bus, 69-bus and 141-bus test systems with Turkish DG and load data were conducted to validate the effectiveness of the proposed approach. The distribution of the Pareto front solutions and the optimal objective functions are compared with the other known algorithms. The simulation results show that the average energy not supplied and annual energy losses for the test systems are reduced by up to 68% and 64%, respectively. Moreover, the Pareto fronts of the proposed method show a better distribution and dominate those obtained by MOGWO, MOSMA, NSGA-II, MOPSO and MOEA-D according to three different Pareto optimization metrics. Finally, the computational effort result shows faster convergence of MOSCA compared to MOGWO, MOSMA, NSGA-II, MOPSO and MOEAD.

1. Introduction

1.1. Motivations

Today, energy supply is one of the most important concerns of planners and designers of energy systems. This issue has become one of the fundamental problems of mankind in the forthcoming years. In electrical distribution networks (EDNs), most of the encountered problems can be solved by proposing proper planning and operation strategies while maintaining system reliability.

The traditional EDNs are composed of radial feeders with laterals through which the customers are supplied. Utilizing radial structure in EDNs has several advantages such as lower fault currents, easy protection and operation control, better voltage regulation, and so on. However, radial EDNs suffer from voltage problems and poor reliability, especially for the customers connected at the end of the feeders. To improve reliability, one can consider proper placement and operation of switches [1] and protection devices to reconfigure the network in case of component failures [2]. Nevertheless, such a reconfiguration itself may not be effective for voltage magnitude problems and network losses. In this context, Energy Storage Systems (ESSs) and Distributed Generators (DGs) may help to reduce the outage durations while minimizing the voltage magnitude problems and network losses, if they are planned adequately [3].

1.2. Literature review

Due to the stochastic nature of the power generated by renewable based DGs such as photovoltaic (PV) and wind turbines (WT), distribution companies need to deploy ESS to mitigate these uncertainties [4]. ESSs provide a shaved peak load profile [5,6] and maximize the intended benefits of DGs, such as reducing losses [7], improving power quality [8], and grid reliability [9]. On the other hand, if the locations of DGs and ESSs are not chosen appropriately, grid reliability may be compromised, power losses may increase, and ultimately lead to higher costs.

* Corresponding author.
E-mail addresses: b.ahmadi@utwente.nl (B. Ahmadi), oguzhan.ceylan@marmara.edu.tr (O. Ceylan), ozdemiraydo@itu.edu.tr (A. Ozdemir), fotuhi@sharif.edu (M. Fotuhi-Firuzabad).

https://doi.org/10.1016/j.apenergy.2022.118887
Received 20 September 2021; Received in revised form 19 February 2022; Accepted 2 March 2022
Available online 22 March 2022

The models used to determine proper optimal or near-optimal planning and operation strategies for the achievement of intended objectives are generally non-linear and non-convex. They are formulated as constrained optimization problems comprising of continuous and integer decision variables [10]. The derivative-based optimization algorithms may suffer from complex derivative computations and get stuck in local minimums [11]. Therefore, heuristic algorithms are generally preferred for solving optimization problems because they provide a fast solution and are easy to understand and implement. Moreover, heuristic algorithms are able to escape from local optima by relying on simple concepts from nature and can be used for a wide variety of problems in different disciplines. The No Free Lunch (NFL) theorem [12] states that a single heuristic algorithm cannot solve all possible optimization problems; therefore, heuristic algorithms must be tuned and implemented for specific problems.

Besides the benefit of an optimal solution found by the heuristic algorithm for integrating DGs and ESSs with EDNs in reducing outage duration and increasing the effective operation of distribution system capacity, there are several advantages in the technical, economic, and environmental impacts of distributed energy resources integration. The work published in [13] focused on integrating WT units and ESSs to reduce distribution losses and customer's energy not supplied as reliability improvement. In [14], to find an optimal allocation of fast-acting ESS units, a continuous-time approach based on coefficients of the Bernstein polynomial was used and compared to existing available strategies. Also, ESSs were implemented in different WT integration applications such as frequency regulation, peak shaving, and ancillary services [15–17].

In order to improve the reliability of EDN, the research studies mainly focused on investigating the role of placement or upgrading of switches and protection devices, determining the optimal system reconfiguration, optimal allocation of DG, and the impact of ESS to improve the overall reliability of the system through the reliability indices [18]. Alam et all proposed a model to determine the optimal placement of reclosers and switches for improving system reliability and minimizing the outage costs [19]. They have also considered the uncertainties in failure rates, load data, and repair rates in the formulation using a three-point estimate method. In determining the optimal placement of reclosers and switches to improve the system reliability and minimize the outage cost considering several uncertainties such as failure and repair rate in [19,20]. In [21], a novel statistical method is provided to estimate the impact of DG units on the reliability, resilience, and economic analysis of the EDNs. In [22], a new hybrid particle swarm optimization-aunt colony optimization algorithm was used to determine the optimal sizes, types, and locations of automatic switching devices/protective devices in MV distribution feeders based on their protective coordination. In [23], a three-state particle swarm optimization approach was presented to determine the optimum number of sectionalizers and breakers and the locations of the units simultaneously in EDNs. In [24], the authors used a genetic algorithm (GA) aiming to improve reliability indices in EDNs and determined the optimal switch locations.

Besides optimal switch allocation, network reconfiguration and network expansion planning were used to improve system reliability. In [25,26], a multi-objective stochastic model was proposed for determining the optimal system reconfiguration and DG allocation. Jangdoost et al. in [27] claimed that the optimal system reconfiguration involving plug-in hybrid electric vehicles improved reliability indices and minimized the operation costs of EDNs. In [28], the authors used the teaching–learning optimization algorithm to find the optimal system reconfiguration to improve the system reliability-based indices such as system average interruption duration index (SAIDI), system average interruption frequency index (SAIFI), and average energy not supplied (AENS).

1.3. Contribution and paper organization

Although there are several efforts reported in the literature with regards to the reliability improvement of active EDNs, most of them were based on the switching/network configuration actions, without considering the other prospective objectives. This study aims at determining optimal planning of DERs in EDNs from a multi-objective optimization perspective. The Pareto optimal solutions are determined to improve the system reliability while minimizing the annual DER costs and power losses. In this regard, optimal location, size, and type of PV and WT units as well as charging/discharging management strategies of ESS units are determined. We utilized and used the modified version of Multi-Objective Sine–cosine Algorithm (MOSCA) [29] as a computational tool reason of which can be summarized as follows. The ability to explore and escape from local minima of single objective SCA is transferred to MOSCA, which, like all other nonderivative-based methods, uses random initial solutions. The algorithm uses sine and cosine functions that exhibit two types of behavior: the ability to explore when the functions take values above 1 or below −1, and the ability to exploit when they are between 1 and −1. Thus, the cyclic pattern of the sine and cosine functions help exploration of the search space. The algorithm uses Pareto dominance concept to compare the solution candidates. Moreover, the implementation of the algorithm is easy due to requirement of adjusting few number of control parameters. The proposed solution algorithm and formulations are implemented and tested on IEEE 33-bus EDN and 69-bus standard test systems. Simulation results are compared with the corresponding base case values to quantify all the benefits obtained from different Pareto solutions. Moreover, Pareto fronts of the proposed methodology are compared with the ones obtained by Multi-Objective Evolutionary Algorithm based on Decomposition (MOEA-D), Multi-Objective Grey Wolf optimizer (MOGWO) [30], Multi-Objective Slime Mould Algorithm (MOSMA) [31], Non-dominated Sorting Genetic Algorithm II (NSGA-II) [32] and Multi-Objective Particle Swarm Optimization (MOPSO) by using different Pareto optimal metrics.

The highlights of the manuscript are as follows:

- Determining optimal planning of DERs and management of ESSs in EDNs using a three-dimensional multi-objective optimization framework.
- Improving the network reliability together with minimizing the power losses and the annual costs.
- Considering 72 h optimization period to take the seasonal characteristics of the load and the DGs into account.
- Utilizing real load curve, and considering wind and solar radiation data of Turkish territory.
- Utilizing a multi-objective sine–cosine algorithm providing better Pareto fronts according to three performance indices.

The structure of the paper is as follows. The statement of the problem including the objective functions and constraints is described in Section 2. Section 3 presents the solution methodology and MOSCA implementation. The results of test system implementations are illustrated in Section 4. Finally, the paper terminates with the conclusions at Section 5.

2. Multi-objective formulation of the problem

This study aims the formulation and solution of a three-dimensional constrained optimization problem through Pareto optimal concept. The objectives are annual energy losses, annual installation and operation costs of DERs, and average energy not served (AENS). The mathematical statement of the problem can be given as;

$$\underset{w.r.t.\ \vec{L},\vec{T},\vec{S},\vec{E},\vec{P},\vec{O}}{\text{minimize}} \{f_{\text{AEL}}, f_{\text{cost}}, f_{\text{AENS}}\} \tag{1}$$

$$\text{subject to } \begin{cases} h_n = 0, & n = 1, 2, \ldots, l \\ g_n \geq 0, & n = 1, 2, \ldots, k \end{cases}$$

where f_{AEL}, f_{cost}, and f_{AENS} are the aforementioned objectives. The terms $\overrightarrow{L}$, $\overrightarrow{T}$, and $\overrightarrow{S}$ denote the locations, the types, and the sizes of different DG units, respectively. $\overrightarrow{L}$, $\overrightarrow{P}$, $\overrightarrow{E}$, and $\overrightarrow{O}$ denote the location, maximum charging/discharging power rates, energy capacity (size), and operational strategy of ESS units, respectively. The terms h_n and g_n show the equality and inequality constraints, respectively.

2.1. Objectives

Details of the objective functions are given below.

2.1.1. Annual energy losses

Real power losses of the jth branch of a distribution network at time i can be calculated using $Pl^i_j = (I^i_j)^2.R_j$, where, R_j is the resistance of the j_{th} branch. Energy losses will be the sum of hourly power losses for an intended period. Annual energy losses (AEL) of a system comprising N_{br} branches would be the sum of hourly losses along a year. It can be expressed as follows:

$$f_{\text{AEL}} = \sum_{i=1}^{N_T} \sum_{j=1}^{N_{br}} Pl^i_j \tag{2}$$

where the optimization period N_T is 365.

2.1.2. Annual investment, maintenance and operation costs

WT and PV plant costs depend on the market strategy and the geographical location for the installment point. Since DG plant costs mostly depend on the power rating of the units but the ESS costs depend on both the power rating and the energy size of the units, it is better to model the costs of ESS and DG separately.

The objective function is mathematically formulated as follows:

$$f_{\text{cost}} = C_{DG} + C_{ESS-E} + C_{ESS-P} \tag{3}$$

$$C_{DG} = \sum_{n=1}^{N_{DG}} (\overline{IC}_{DG} \times C_{\tau_{DG}} + \overline{O\&M}_{DG}) \times S_{DG_n} \tag{4}$$

$$C_{ESS-E} = \sum_{n=1}^{N_{ESS}} (\overline{IC}_{BE} \times C_{\tau_B} + \overline{O\&M}_{Bv}) \times E_{ESS_n} \tag{5}$$

$$C_{ESS-P} = \sum_{n=1}^{N_{ESS}} (\overline{IC}_{BP} \times C_{\tau_B} + \overline{O\&M}_{Bf}) \times P_{ESS_n} \tag{6}$$

$$C_\tau = \frac{r(1+r)^\tau}{(1+r)^\tau - 1} \tag{7}$$

where C_{DG}, C_{ESS-E}, and C_{ESS-P} are the expressed DGs costs, ESSs energy costs, and ESSs power rating costs. The term of $\overline{IC}$ used for presenting the units investment cost in USD/kW or USD/kWh; whereas $\overline{O\&M}$ shows the units annual maintenance and operation costs in USD/kW-yr or USD/kWh-yr. The estimated lifetime of the DG and ESS units in years shown with τ, P_{ESS} and E_{ESS} are the maximum charging/discharging power rate and the rated state of charge of the ESS units, and S_{DG} is the DGs installed size. Regarding the maintenance and operation costs of the ESSs, the subscripts v and f denote the variable and the fixed maintenance and operation costs, respectively. The number of ESS units (N_{ESS}) and the DG units (N_{DG}) are determined through the optimization process. In Eq. (7), C_τ represent the DG and ESS units capacity recovery factor, with an interest rate of r. Table 1 shows all the parameters used for modeling the DG and ESS units costs.

Table 1
ESS and DG units parameters [33–35].

Parameter:	Value	Units
τ_{PV}	30	year
τ_{WT}	25	year
$\overline{IC}_{PV}$	1830	$/kW
$\overline{IC}_{WT}$	1600	$/kW
$\overline{O\&M}_{PV}$	18	$/kW-year
$\overline{O\&M}_{WT}$	25	$/kW-year
τ_B	10	year
$\overline{IC}_{BE}$	160	$/kWh
$\overline{IC}_{BP}$	1800	$/kW
$\overline{O\&M}_{Bf}$	10	$/kW-year
$\overline{OM}_{Bv}$	0.03	$/kWh-year

2.1.3. Reliability

In radial EDNs, a load connected to a bus can be supplied if all the components between the supply point and the mentioned bus are operating. Hence, load point reliability indices can be calculated using the component reliability parameters of the serially connected components along the load–supply chain [36]. Component reliability parameters are determined using the outage statistic data for the failure rate (λ) and the average outage time (r) of the components.

There are a number of reliability indices that can be calculated in EDNs and they are generally categorized into two groups, namely, system-oriented and customer-oriented indices [36]. In this paper, average energy not served (AENS) is used as the reliability index, which is defined as:

$$f_{\text{AENS}} = \frac{\sum_{k=1}^{N_{bus}} L_k U_k}{\sum_{k=1}^{N_{bus}} N_k} \tag{8}$$

where L_k is the average load connected to the kth load point, N_k is the number of costumers at load point or bus k, and U_k is the annual outage time which is defined as $U_k = \lambda_k \times r_k$.

2.2. Constraints

Equality and inequality constraints comprising of power balance equations and technical restrictions of the electrical variables are described below.

1. Power balance constraint:

$$\begin{cases} P^i_{\text{MG}} + P^i_{\text{DG}} + P^i_{\text{ESSD}} = P^i_{\text{load}} + P^i_{\text{ESSC}} + P^i_{\text{losses}} \\ Q^i_{\text{MG}} = Q^i_{\text{load}} + Q^i_{\text{losses}} \\ \forall i \in N_{\text{T}} \end{cases} \tag{9}$$

   where P_{MG} and P_{DG} represent the active power supplied from the main grid and DG units, Q_{MG} is reactive power provided by the main grid. The discharge powers and charge powers of ESS units denoted by P_{ESSD} and P_{ESSC}. The active and reactive losses and load shown by Q_{load}, Q_{losses}, P_{load}, and Q_{losses}, respectively.
2. Bus voltage magnitude limits: In order to maintain power quality, the node voltages should be within operation limits as shown below.

$$V^{i,\min}_j \leq V^i_j \leq V^{i,\max}_j \quad \forall i \in N_{\text{T}}, j \in N_{\text{Bus}} \tag{10}$$

   where the values of $V^{i,\max}_j$ and $V^{i,\min}_j$ are 1.05 p.u. and 0.95 p.u., respectively
3. Generation constraints:

$$\begin{cases} P^i_{\text{MG}} \leq P_{\text{MG}_{max}} \\ Q^i_{\text{MG}} \leq Q_{\text{MG}_{max}} \\ \forall i \in N_{\text{T}} \end{cases} \tag{11}$$

$$P_{\text{DG}} \leq 1\,\text{MW} \tag{12}$$

4. Storage constraints:

$$\begin{cases} E_{ESS} \le 1\,\text{MWh} \\ (P^i_{ESSC}, P^i_{ESSD}) \le 1\,\text{MW} \\ 0.2 * E_{ESS} \le SoC^i_{ESS} \le 0.8 * E_{ESS} \\ \forall i \in N_T \end{cases} \tag{13}$$

where state of charge(SoC) of the ESS for each time step shown with SoC^i_{ESS}.
Note that the charging and discharging phases of ESS units are identical at each time interval to avoid the internal energy exchange between ESS units.

3. Solution methodology

3.1. Constrained multi-objective optimization problems

The mathematical formulation for an n-dimensional multi-objective optimization can be given as follows:

$$\underset{w.r.t\ \vec{x}}{\text{minimize}}\ F(\vec{x}) = [f_1(\vec{x}), f_2(\vec{x}), f_3(\vec{x}), \dots, f_n(\vec{x})] \tag{14}$$

$$\vec{x} = \{x_1, x_2, \dots, x_d\}$$

$$Subject\quad to \begin{cases} g_t(\vec{x}) \ge 0, \quad t = 1, 2, \dots, k \\ h_t(\vec{x}) = 0, \quad t = 1, 2, \dots, l \\ \vec{x}^{lb} \le \vec{x} \le \vec{x}^{ub} \end{cases}$$

where a set of solutions can be found for n individual objective functions that each solution includes d variables between the $(\vec{x})^{lb}$ and $(\vec{x})^{ub}$ bounds as an acceptable trade-off instead of an optimal solution. The optimal solutions can be characterized by dominance relation and can also be referred as Pareto efficiency or optimality as defined in [37].

3.2. Multi-objective sine–cosine algorithm

The single objective sine–cosine algorithm (SCA) is a novel population-based method that starts searching for the optimal solution with a random set of solutions [38]. The two different mathematical formulations are used to evaluate each solution to balance exploitation and exploration phases for the process. These expressions are given as:

$$X_d^{t+1} = \begin{cases} X_d^t + A \sin(2\pi r_1) \times D & if \quad r_3 \ge 0.5 \\ X_d^t + A \cos(2\pi r_1) \times D & if \quad r_3 < 0.5 \end{cases} \tag{15}$$

$$D = |r_2 X b_d^t - X_d^t| \tag{16}$$

$$A = a - a(\frac{t}{t_{max}})$$

where X_d^t is the dth solution variable in iteration-t and Xb shows the best solution of the population. In the above equations r_1, r_2, and r_3 are random numbers generated between 0 and 1 and the terms a is constant numbers and sets to 2. These parameters are used for controlling the solution to go through the exploration or exploitation phases.

The cyclic pattern of sinusoidal functions allows for re-positioning of the solution variables around another solution (the optimal solution in the current iteration) and guarantees the exploitation of the search space. For exploring the search space, the solutions should be able to explore the outside of the space by changing the range of the sine and cosine functions.

For multi-objective optimization problems, Pareto optimal dominance is proposed to find non-dominated solutions. Some definitions regarding the Pareto front solution concept are first summarized below for a better understanding of the subject [29]:

Let us define two solution vectors: $\vec{a} = \{a_1, a_2, a_3, \dots, a_k\}$ and $\vec{b} = \{b_1, b_2, \dots, b_k\}$,

Definition 1 (*Pareto Dominance*)**.** The solution $\vec{a}$ dominates $\vec{b}$, denoted as $a > b$, if:

$$\forall i\{1, 2, 3, \dots, k\}, \left[f\left(a_i\right) \geqslant f\left(b_i\right)\right] \wedge \left[i \in 1, 2, 3, \dots, k : f\left(x_i\right)\right] \tag{17}$$

Definition 2 (*Pareto Optimality*)**.** The solution $\vec{a} \in X$ is a Pareto optimal solution if:

$$\nexists \vec{b} \in X \mid F(\vec{b}) > F(\vec{a}) \tag{18}$$

The two solutions are non-dominated solutions to each other if neither of two solutions dominates the other one.

Definition 3 (*Pareto Optimal Set (Archive Set)*)**.** The set with all the non-dominated solutions is called the Pareto set:

$$P_s := \{a, b \in X \mid \exists F(b) > F(a)\} \tag{19}$$

Definition 4 (*Pareto Optimal Front*)**.** The set with the corresponding objective values of the Pareto solutions in the archive set is called the Pareto optimal front:

$$P_f := \{F(a) \mid a \in P_s\} \tag{20}$$

P_f is referred as an 'archive', which is used to store all the non-dominated Pareto solutions during the iterative process of optimization algorithm. Furthermore, two mechanisms are employed to increase the distribution of the solutions since the number of the solutions in the archive is fixed. Firstly, a roulette-wheel mechanism with a probability value of P_i (Shown in Eq. (21)) is used for selecting the new solutions among the solutions in the least populated area (neighborhood) to improve the distribution of the Pareto optimal front.

$$P_i = \frac{c}{N_i} \tag{21}$$

where N_i represents the number of solutions in the vicinity of the ith solution and c is a constant value.

The second mechanism is used when the archive is full. The solutions with the most populated neighborhoods are removed and the new non-dominated solutions are added to the archive. The roulette-wheel mechanism used for selecting the solutions with a probability of P_i:

$$P_i = \frac{N_i}{c} \quad , c > 1 \tag{22}$$

The other proposed rules for updating the solution of the archive are as follows. Suppose that none of the archive members or a new generated solution dominates each other or a new generated solution dominates one or more archive members. In that case, the new solution is included in the archive, and the dominated ones are removed.

A dynamic stopping criterion is added to the algorithm to find more accurate Pareto solutions. The dynamic stopping criterion uses the C index [39] of the obtained solutions and will be explained in 4.4. The percentage of domination of the solutions at each iteration is compared to the predefined iteration number before. The optimization process is stopped if the percentage is small enough. The mathematical formulation of the stopping criteria applied to the process is given in Eq. (23).

$$B_{stop} = \begin{cases} 1 & if \quad |C(n, n-\Delta)| < \epsilon \\ 0 & otherwise \end{cases} \tag{23}$$

where B_{stop} is a binary variable used for the stopping process, ϵ denote a small number sets as a tolerance, n and Δ represent the current iteration number and a predefined integer value for comparing the solutions using C index.

3.3. Implementation of MOSCA into the problem

The steps of the proposed MOSCA algorithm to determine the Pareto fronts comprising near-optimal DG sizes, types, and sites and ESS powers, energies, and state of charges are illustrated in Algorithm 1 (see [40] for Forward-backward sweep calculation).

Algorithm 1: MOSCA

```
Set the basic parameters of algorithm;
Set the input parameters of DGs, ESSs, DNs;
Initialize the solutions vector (x_i) randomly;
Create the empty archive repository;
while t ≤ t_max do
    for each solution do
        Check the boundaries of search agent position variables
          using proposed method [5];
        Calculate the objective values of the solutions (F_i)
          through the Forward-backward sweep calculation [40]
          and analytic calculation of reliability measurement;
        Update the archive with the non-dominated solutions;
    end
    if the number of archive solutions exceed the maximum archive
      size then
        Omit the solutions with high density population in the
          neighborhood;
    end
    Choose the Xb randomly from the set of archive solution;
    for each solution do
        Update r_1, r_2, and r_3;
        Update the solution position (X_j) using (15)
    end
    t = t + 1;
    if secondary stopping criteria satisfied then
        stop the loop;
    end
end
Return the archive fitness and solutions vectors;
```

4. Case studies and results

4.1. Test systems data

The proposed formulations are applied on IEEE 33-bus, 69-bus, and 141-bus EDNs. Feeder data of the test systems are taken from [41,42], and [43]. Reliability data, load types, and the number of customers at each bus are extracted from Table 11 in the Appendix for 141-bus system, [44,45] for 33-bus and 69-bus system. Optimization period is selected as 72 h (24 h for each representative summer, winter and spring/fall day) to account the seasonal effects.

At first, base-case load flow calculations are performed for the test systems without any DER sources. Active power losses at peak load conditions (3.7 MW) is found to be 201.9 kW for IEEE 33-bus test system. Similarly, 69-bus test system showed 224.5 kW of active power losses at a peak load of 3.8 MW and 550.4 kW power losses for 141-bus system with 11.1 MW peak load.

Two different failure rates are assigned to the branches in the system. λ_l denotes the main feeder branches' failure rate between the busbars, and λ_d denotes the laterals' failure rates between the busbars and the loads. Both failure rates are assumed to be proportional to the length of the branches. On the other hand, the main branches and laterals' average repair time are assumed to be 4 h and 2 h, respectively. The residential, commercial, and industrial loads' hourly load characteristics are shown in Fig. 1.

4.2. DGs and ESS outputs

One-year solar irradiation and wind speed data for a specific district in Turkey [46,47] were used to calculate the WT and PV outputs. Since the locations of DG units are close to each other (at the same feeder), we used the same output patterns given in [46,47] for all WTs and PVs. Mean capacity factors for WT and PV units were found as 35% and 34%, respectively. The DG outputs are illustrated in Figs. 2 and 3.

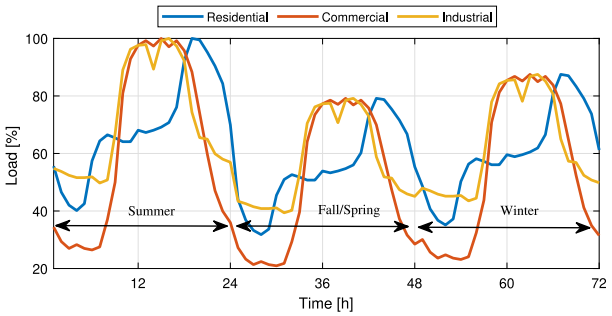

Fig. 1. Scaled hourly loads.

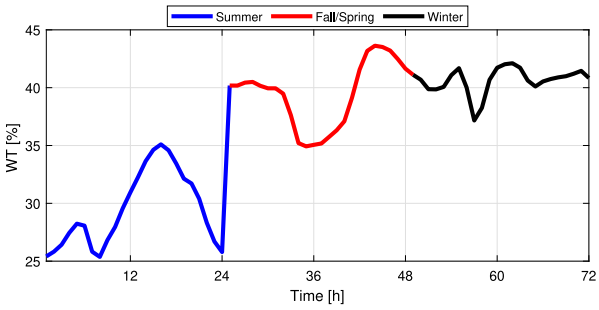

Fig. 2. Estimated scaled WT outputs.

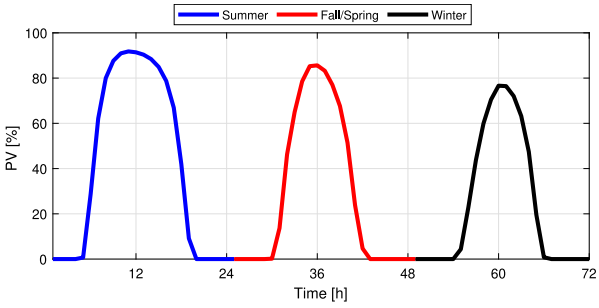

Fig. 3. Estimated scaled PV outputs.

4.3. Results and discussion

The results are discussed in this section from the point of intended objectives and Pareto front characteristics. Among the three basic objectives, priority is given to the system reliability, which is quantified by AENS. The Pareto optimal solution of the proposed objective function is determined using the MOSCA for the three case studies of 33-bus, 69-bus, and 141-bus systems.

We ran the MOSCA algorithms on a PC with 16 GB RAM, an Intel Core i7-7700 3.6 GHz processor configuration, and MATLAB version 2020b. For each case study, the solution that has the smallest distance to the origin of the 3-dimensional objective space is set as the candidate Pareto solution (CPS). The results of CPS are highlighted and compared with the values of the base case to evaluate the benefits of the optimization process. We have also included the flowchart of the process for the mentioned formulation in Fig. 4.

4.3.1. Case study I

The Pareto solutions of the optimization problem formulated in Eq. (1) are determined using MOSCA for 33-bus test system. The

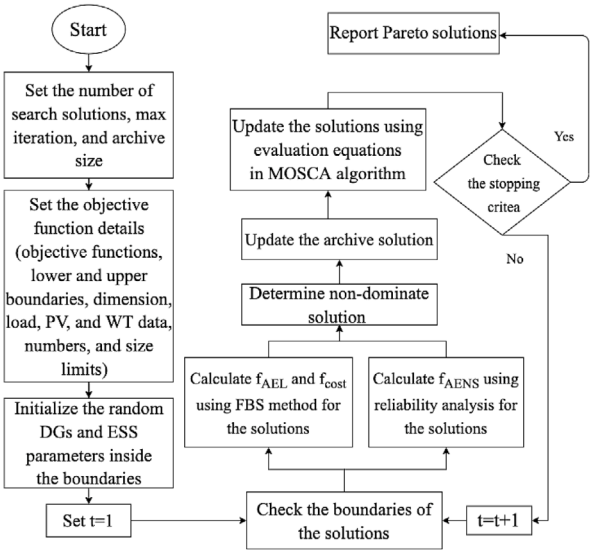

Fig. 4. The flowchart of finding the optimal Pareto solutions for the proposed formulation.

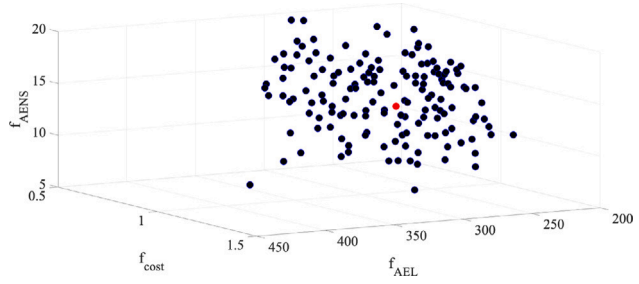

Fig. 5. Pareto optimal solution for Case Study I.

resulting non-dominated Pareto solution of ten independent trials are shown in Fig. 5 where the red one denotes the CPS.

The annual energy losses for the Pareto solutions are between 227 and 406 MWh, which was 623 MWh for the base case operating conditions. The base case AENS value of 24.48 kWh/customer reduces to the range of 7.76 to 19.72 kWh/customer by the Pareto optimal solutions.

Optimal parameters for the CPS are illustrated in Table 2. It comprises of five WTs, one PV, and 6 ESS units. The total DG capacity and ESS size are 3920 kW and 3250 kWh, respectively. The total DER cost of the CPS is 0.8 MSD. On the other hand, it reduces the energy losses to 248 MWh, corresponding to 60.1% of the base case losses. AENS reductions of Pareto solution candidate (PSC) is almost 50.8%. Hourly power losses for the base conditions and the PSC are shown in Fig. 6. It is clear that the loss reductions are more remarkable for higher load levels (peak load durations). For example, peak load power losses reduce from 173.3 kW to 76.3 kW (57.0%). Note that the ratio between the peak load and the minimum load decreases due to effective peak shaving of ESS units. ESS units SoC along the simulation period shown in Fig. 7.

The final discussion is on bus voltage magnitudes. Among several undervoltage problems for the base case operating conditions, the most critical one is 0.9189 p.u. at bus number 18 at hour 6 p.m. in a summer day. All the Pareto solutions have fixed all the undervoltage problems and the minimum bus voltage magnitudes were improved to a range between 0.9501 and 0.9660 p.u. The minimum bus voltage magnitude for the CPS is 0.9549 p.u. at bus 18 on a summer day at 7 p.m. Bus voltage profiles for the CPS configuration are illustrated

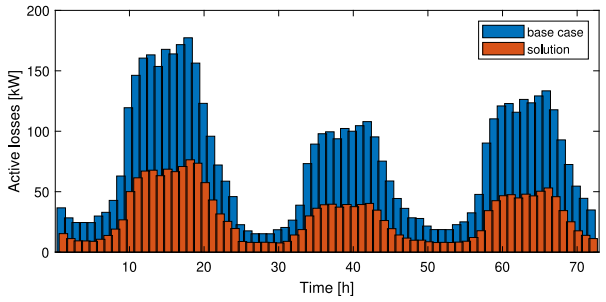

Fig. 6. Hourly loss reductions in 33-bus test system for the CPS.

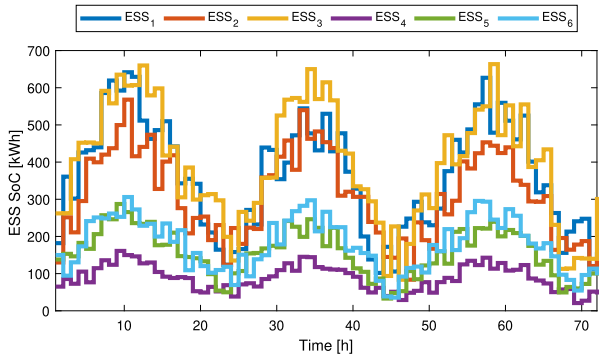

Fig. 7. SoC for ESS units in IEEE 33-bus test system for the CPS.

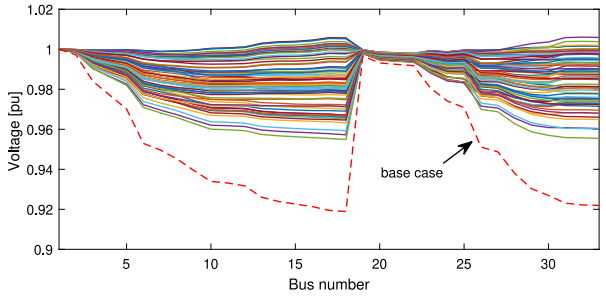

Fig. 8. Voltage magnitude profiles in 33-bus test system for the CPS and the base case (6 p.m. of the summer day).

Table 2
ESS and DG parameters for candidate Pareto solution.

#	DG			ESS		
	Location	Size [kW]	Type	Location	Energy [kWh]	Power [kW]
1	14	500	WT	9	680	62
2	17	500	WT	15	800	73
3	25	1000	WT	22	860	78
4	29	500	WT	24	190	17
5	31	640	PV	25	340	31
6	32	780	WT	32	390	35

in Fig. 8 together with the worst ones in the base case (6 p.m. of the summer day). Note that each characteristic shows the voltage profiles at different hours of three representative days.

4.3.2. Case study II

The non-dominated Pareto solutions of ten independent optimization trials in 69-bus test system are shown in Fig. 9. The red one denotes the CPS. The resulting objective functions of the Pareto solutions are illustrated in Table 3 together with the minimum voltage magnitude. The result shows that the Pareto solutions with the installation of

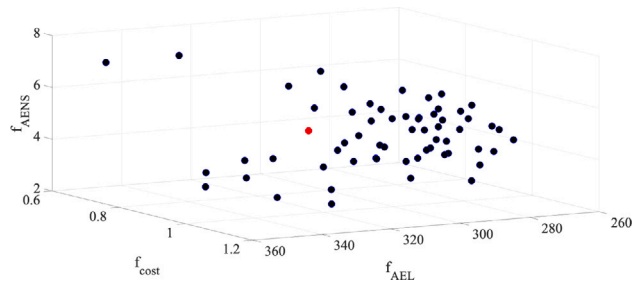

Fig. 9. Pareto optimal solution for Case Study II.

Table 3
Objective function values of the Pareto solutions for 69-bus test system.

	Pareto solutions		Base case
	min	max	
AEL (MWh)	264	352	738
AENS (kWh)	2.81	7.06	7.82
COST (MUSD)	0.65	1.17	
Minimum voltage magnitude (p.u.)	0.95	0.96	0.91

Table 4
ESS and DG parameters in 69-bus test system for the CPS.

#	DG			ESS		
	Location	Size [kW]	Type	Location	Energy [kWh]	Power [kW]
1	14	500	WT	12	680	94
2	16	370	WT	21	740	102
3	58	840	WT	25	620	86
4	62	290	WT	46	600	83
5	64	680	WT			
6	65	1000	PV			

proper ESS and DG units reduce the annual energy losses up to 64.2%. On the other hand the Pareto solutions reduce the amount of energy not-supplied up to 64%.

The CPS with 0.75 MUSD annual DG and ESS cost includes 6 DGs and 4 ESS units. Table 4 presents the optimal DG and ESS locations and sizes. The results show that 1 PV and 5 WTs are the best numbers of different DG types. The total DG size in CPS is 3.68 MW, and the total ESSs capacity is 2.64 MWh. The CPS reduces the annual energy losses by 59.3% compared to the 738 MWh annual losses in the base case. Hourly power losses and SoC of ESS units are shown for the two operating conditions in Figs. 10 and 11, respectively. One can easily recognize that the loss reductions are more remarkable for higher load levels. It indicates an effective peak shaving due to the operation management of ESS units.

Finally, the voltage profiles provided by CPS are compared with the base case ones in Fig. 12. Note that the voltage profiles for the base case operating conditions are given only for summer - 4 p.m., as being the most critical one. The minimum voltage magnitude is 0.916 p.u. at bus 65. It is improved to 0.957 p.u. by the CPS.

4.3.3. Case study III

The obtained Pareto front solutions for 141 bus system with over 63% improvement in annual energy losses and up to 40% improvement in AENS value are shown in Fig. 13. Table 5 illustrates the summary of the achieved improvement for the Pareto solutions. The ESS and DG parameters for CPS are listed in Table 6. Note that CPS is shown with a red dot in Fig. 13.

The hourly losses of the system, SoC of the ESS units and the voltage magnitudes are illustrated in Fig. 14, 16, and 15, respectively. One can realize that there are some slight shifts in the peak periods and almost 57% loss reductions in Fig. 14. Optimal control strategy for the ESS units provide a 1.3 MWh of energy exchange between peak and off-peak hours per day. Finally, the minimum voltage magnitude of 0.93 p.u. (bus 87) for the base case operating conditions is improved to 0.95 p.u. (bus 52) for the CPS.

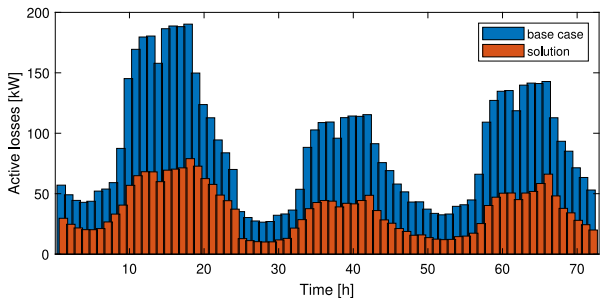

Fig. 10. Hourly loss reductions in 69-bus test system for the CPS.

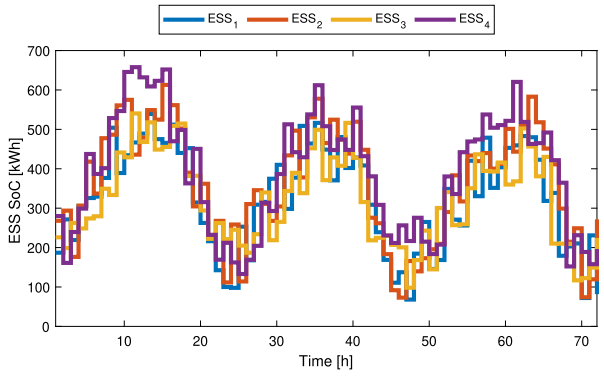

Fig. 11. ESS's SoC in 69-bus test system for the CPS.

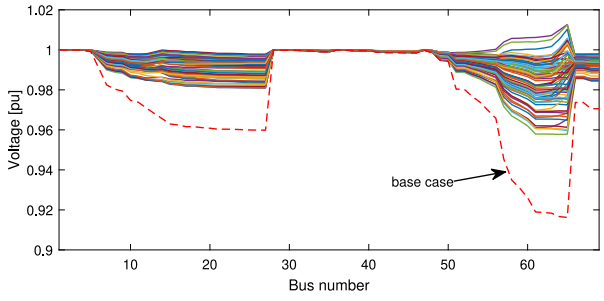

Fig. 12. Voltage magnitude profiles in 69-bus test system for the CPS and the base case (6 p.m. of the summer day).

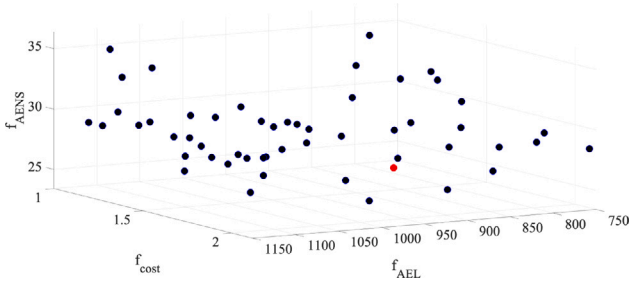

Fig. 13. Pareto optimal solution for Case Study III.

4.4. Comparison of the solution algorithms

The quality of the non-dominated Pareto solutions obtained by the proposed algorithm is measured and compared with those of the

Table 5
Objective function values of the Pareto solutions for 141-bus test system.

	Pareto solutions		Base case
	min	max	
AEL (MWh)	111	757	2083
AENS (kWh)	23.4	36.3	39.3
COST (MUSD)	1.03	2.11	
Minimum voltage magnitude (p.u.)	0.95	0.96	0.93

Table 6
ESS and DG parameters in 141-bus test system for the CPS.

#	DG			ESS		
	Location	Size [kW]	Type	Location	Energy [kWh]	Power [kW]
1	61	800	WT	60	370	31
2	67	580	WT	65	940	99
3	72	860	WT	71	600	63
4	75	840	PV	83	750	78
5	77	240	PV			
6	78	900	PV			
7	79	920	WT			
8	82	810	WT			
9	83	1000	WT			
10	84	510	WT			
11	85	410	WT			
12	94	900	WT			
13	109	780	WT			
14	115	490	PV			

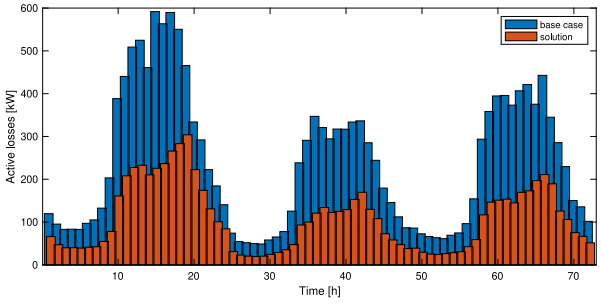

Fig. 14. Hourly losses reductions in 141-bus test system for the CPS.

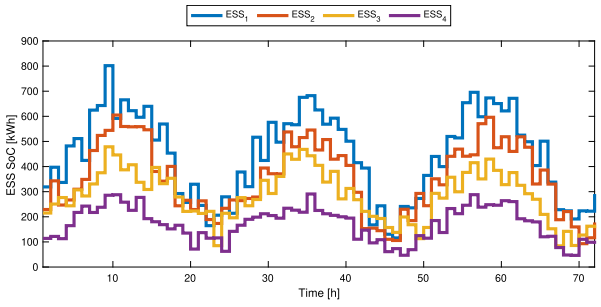

Fig. 15. ESS's SoC in 141-bus test system for the CPS.

MOGWO, MOSMA, NSGA-II, MOEA-D and MOPSO algorithms by using several performance metrics, namely the spacing metric (SM), the C-index metric [48], Hypervolume (HV) [49–51] and the computational burden for the solutions. For a fair comparison, we set the parameters of MOPSO, MOEA-D, MOGWO, MOSMA, and NSGA-II to the values given in Table 7, where n in MOEA-D algorithm is the number of population. We analyzed the impacts of the different algorithmic parameters of methods on the solution performance in terms of C-index values. The results show that the algorithmic parameters of MOPSO, NSGA-II and MOEA-D solutions are the best parameters for comparison. For the methods, the population count was set to 100 and

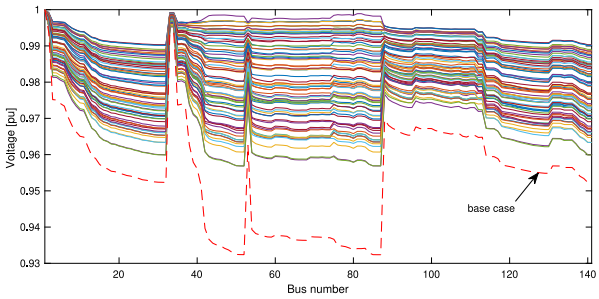

Fig. 16. Voltage magnitude profiles in 141-bus test system for the CPS and the base case (6 p.m. of a summer day).

Table 7
Parameters of NSGA-II, MOPSO, and MOEA-D.

Method	Parameter	Value
MOPSO	Grid inflation rate	0.1
	Personal learning coefficient (c1)	1.0
	Global learning coefficient (c2)	1.0
	Number of grids per dimension	10.0
	Leader selection parameter	4.0
	Damping ratio	0.95
MOEA-D	Scaling factor	0.5
	Crossover rate	1.0
	Scale parameter (η)	20
	Mutation probability	1/n
NSGA-II	Crossover probability	0.9
	Mutation probability	0.5
	Mutation strength	0.05

the maximum archive count was set to 200. Note that we optimized all these parameters before making the comparisons.

4.4.1. The spacing metric

The SM evaluates the distribution of vectors throughout the set of non-dominated Pareto solutions and calculates with a relative distance measure between consecutive solutions in the archived solutions. Assume that $f_k^n(x)$ is the kth objective function corresponding to nth solution inside the archive set, where k is in between 1 and m and n is in between 1 and t. The minimum Euclidean distance between the two non-dominated solutions-i and -j, can be determined as:

$$d_k = min\Big\{\sum_{k=1}^{m} |f_k^i(x) - f_k^j(x)|\Big\},\ j \neq i,\ j = 1, 2, \ldots, t \tag{24}$$

Moreover the distance found in the Eq. (24) can be normalized by using the maximum Euclidean distance in the set ($[f_{\{m-max\}} - f_{\{m-min\}}]$). Spacing is defined as the standard deviation of those minimum Euclidean distances as given;

$$S = \Big(\frac{1}{t}\sum_{i=1}^{t}(\bar{d} - d_i)^2\Big)^{\frac{1}{2}} \tag{25}$$

where $\bar{d}$ is the average Euclidean distance between the solutions.

Note that the smaller SM value corresponding to closely-distributed non-dominated solutions are better.

Box plots of the SM values for the algorithms are shown in Fig. 17, where each box contains the SM distribution of ten independent trials. Compared to the MOGWO, MOSMA, NSGA-II, MOPSO, and MOEA-D algorithms, the SM distribution of the proposed MOSCA algorithm has the lowest median and dispersion. This indicates that MOSCA performs better than the other algorithms in finding uniformly distributed Pareto solutions and that thereafter MOEA-D found better SM values.

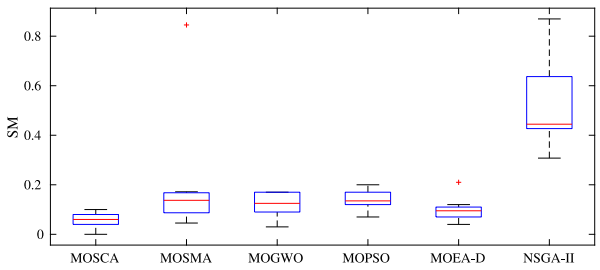

Fig. 17. The box-plots of SM values of different optimization methods.

Table 8
C index-based comparisons of the solution algorithms.

C index	Mean	STD	Maximum	Minimum
C(MOSCA,MOPSO)	3.0	14.2	58.7	0.0
C(MOPSO,MOSCA)	62.7	30.7	100	11.2
C(MOSCA,MOEA-D)	6.3	7.1	27.7	0.0
C(MOEA-D,MOSCA)	54.9	28.5	100	0.0
C(MOSCA,MOGWO)	44.6	43.3	100	0.0
C(MOGWO,MOSCA)	67.8	36.3	100	0.0
C(MOSCA,NSGA-II)	9.8	12.6	52.0	0.0
C(NSGA-II,MOSCA)	61.9	40.2	100	0.0
C(MOSCA,MOSMA)	33.1	37.7	93	0.0
C(MOSMA,MOSCA)	97.1	4.5	100	80

4.4.2. C-index metric

For definition of C index, assume that set_1 and set_2 are the two sets of Pareto solutions. The C index, $C(set_1, set_2)$ refers to the mapping between the ordered pair (set_1, set_2) to the interval [0, 100] percent and it can be calculated as:

$$C(set_1, set_2) := \frac{|\{s_2 \in set_2; \exists s_1 \in set_1 : s_1 \preceq s_2\}|}{|set_2|} \times 100 \tag{26}$$

where s_1, and s_2 are the near-Pareto optimal solutions in set_1, and set_2. The C value shows the percentage of solutions in set_2 that are dominated by near- Pareto optimal solutions in set set_1. Since, $C(set_1, set_2)$ may not be equivalent to $(100 - C(set_2, set_1))$, both $C(set_1, set_2)$ and $C(set_2, set_1)$ have to be calculated for better understanding of dominance of the solutions.

The C index values for the obtained Pareto solutions in all three test systems are shown in Table 8. It is clear that the solutions obtained by MOSCA dominate more than 62%, 54%, 67%, 61% and 97% of the solutions obtained by MOPSO, MOEA-D, MOGWO, NSGA-II, and MOSMA algorithms, respectively. This shows that the MOSCA found better near-Pareto optimal front solutions than other algorithms.

4.4.3. Hypervolume metric

Hypervolume (HV) was originally proposed for comparing the performance of multi-objective evolutionary algorithms (MOEAs) [52]. It computes the volume dominated by a given set of non-dominated solutions bounded by a reference point R. The index HV for a set of non-dominated solutions gives us a clear idea of the convergence and diversity of the set. The HV for a set of solutions called set_1 that normalizes the objective values is defined as:

$$HV(set_1, R) = volume(\bigcup_{i=1}^{|set_1|} v_i) \tag{27}$$

where R is the reference point and is chosen as the maximum value for the normalized objective values. v is the hypercube whose corners are the R and all solutions in set_1. For an illustration of HV for a three-dimensional space, see Fig. 18. Higher values of HV mean that the solution set is closer to an optimal Pareto set and may also indicate a more uniform distribution of solutions in the objective space.

Comparison of the HV index for two sets of non-dominated solutions shows that a set that dominates another set (completely or partially) has a better (higher) HV value. The mean and standard deviations of the HV index found for the different methods are shown in Table 9. The results are obtained by setting R to (1,1,1) for f_{AENS}, f_{cost}, and f_{AEL} and normalizing the Pareto solution values. The purpose of normalizing the values is to put the Pareto front solution found for different test systems on the same scale and to have a general comparison for all algorithms. The result of the HV index shows that MOSCA found a higher value and therefore a better solution quality than the other solutions, and that MOGWO found a better HV value in second place.

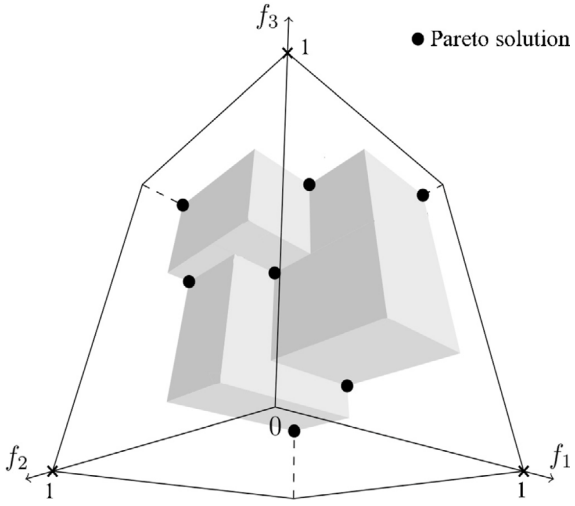

Fig. 18. The estimated HV for 3-D space.

Table 9
The mean and standard deviations of HV values for the algorithms.

	MOSCA	MOSMA	MOGWO	MOPSO	MOEA-D	NSGA-II
Mean	0.838	0.772	0.83	0.794	0.762	0.786
STD	0.045	0.022	0.047	0.017	0.033	0.018

Table 10
The number of iterations and execution times for the methods used.

Case study	Method	# iteration		Execution time [s]	
#		Mean	STD	Mean	STD
I	MOSCA	2684	55	4162	104
I	MOPSO	3019	519	4680	804
I	MOEA-D	5000	0	7940	59
I	MOSMA	5000	0	6180	126
I	MOGWO	2980	412	4361	609
I	NSGA-II	5000	0	10 615	430
II	MOSCA	2546	101	6216	251
II	MOPSO	5000	0	12 183	318
II	MOEA-D	5000	0	12 208	179
II	MOSMA	5000	0	10 991	98
II	MOGWO	4170	704	10 421	1018
II	NSGA-II	5000	0	16 681	270
III	MOSCA	4998	80	84 696	1273
III	MOPSO	5000	0	84 536	164
III	MOEA-D	5000	0	84 770	201
III	MOSMA	5000	0	83 460	882
III	MOGWO	5000	0	85 317	1018
III	NSGA-II	5000	0	89 100	1061

4.4.4. Computational burden

Table 10 compares the mean and standard deviation of the iteration count and execution time for the algorithms. The results of HV, C and S measurements show the better quality of the solutions obtained by MOSCA and the execution time results show that MOSCA converges faster compared to other algorithms. Since the optimization problem depends on the computation time of the power flow, an increase in the

execution time is observed as the size of the test system increases for all tested algorithms.

5. Summary and conclusion

This study has presented optimal planning of DERs in EDNs from a multi-objective optimization perspective, in which the Pareto optimal solutions were determined to improve the system reliability while minimizing the annual DER costs and power losses. In this regard, optimal location, size, and type of DERs along with charging/discharging management strategies of ESS units were determined. An improved multi-objective Sine–cosine Algorithm was used as a computational tool. The proposed formulation and the solution algorithm were implemented and tested on IEEE 33-bus, 69-bus, and 141-bus EDNs.

Simulation results were compared with the corresponding base case values to quantify the range of accomplished benefits with the Pareto solutions. The results show that the Pareto solutions improved the system's AENS index compared to the base case EDNs in between 20% to 68% in the 33-bus system. This improvement for the 69-bus system is in between 10% and 64% and for the 141-bus network in between 7% to 40%, respectively.

The ESS and DG parameters and the benefits of the solution for a Pareto solution with the minimum distance from the origin of objective space were assigned as the candidate Pareto solution (CPS) and analyzed. Comparison of the objective functions and voltage magnitude profiles of CPS to the base case ones showed that annual energy losses were reduced by up to 60%, 55%, and 63% in the case studies, respectively.

Moreover, Pareto fronts of the proposed methodology were compared to those obtained by MOGWO, MOSMA, NSGA-II, MOPSO and MOEA-D using three different Pareto optimal metrics. SM results show that the Pareto fronts of the proposed method distribute more evenly, providing fewer median values. On the other hand, HV and C-metric comparison shows that the Pareto fronts of the proposed solution method dominate most of the Pareto fronts obtained with the other heuristic methods. The HV, SM and C-metric show the better quality of the Pareto solution obtained by MOSCA. In addition to the better quality of the solutions, the computational burden result shows faster convergence of MOSCA compared to other methods. In future studies, we plan to solve multi-objective optimization problems using parallel computing techniques to speed up the search for Pareto solutions and to study the optimal system's restoration process after a blackout.

CRediT authorship contribution statement

Bahman Ahmadi: Investigation, Software development, Writing – original draft, Visualization. **Oguzhan Ceylan:** Methodology, Data curation, Writing – review & editing, Formal analysis. **Aydogan Ozdemir:** Conceptualization, Writing – review & editing, Validation, Supervision, Project administration. **Mahmoud Fotuhi-Firuzabad:** Writing – review & editing, Supervision.

Declaration of competing interest

The authors declare that they have no known competing financial interests or personal relationships that could have appeared to influence the work reported in this paper.

Acknowledgment

This work is funded by the Scientific and Technological Research Council of Turkey (TUBITAK), through 1001 - The Scientific and Technological Research Projects Funding Program under Grant 117E773.

Appendix

see Table 11.

Table 11
141-bus system data.

Branch number	Sending node	Receiving node	R (Ω)	X (Ω)	Active load (kW)	Reactive load (kvar)	Load type	λ_l	λ_d
1	1	2	0.0580	0.0411	0	0	Residential	0.18	0.12
2	2	3	0.1733	0.1229	0	0	Residential	0.48	0.32
3	3	4	0.0009	0.0006	0	0	Residential	0.06	0.04
4	4	5	0.0092	0.0065	0	0	Residential	0.06	0.04
5	5	6	0.0068	0.0049	0	0	Residential	0.06	0.04
6	6	7	0.0471	0.0628	0	0	Residential	0.18	0.12
7	7	8	0.0740	0.0986	64	39.5	Residential	0.24	0.16
8	8	9	0.0652	0.0461	8	5.3	Residential	0.24	0.16
9	9	10	0.0509	0.0361	0	0	Residential	0.18	0.12
10	10	11	0.0117	0.0082	0	0	Residential	0.12	0.08
11	11	12	0.1297	0.0917	21	13.2	Residential	0.42	0.28
12	12	13	0.1233	0.0870	64	39.5	Residential	0.36	0.24
13	13	14	0.0490	0.0347	0	0	Residential	0.18	0.12
14	14	15	0.0962	0.0680	0	0	Residential	0.3	0.2
15	15	16	0.0864	0.0612	0	0	Residential	0.3	0.2
16	16	17	0.0400	0.0283	127	79	Commercial	0.18	0.12
17	17	18	0.0832	0.0569	0	0	Residential	0.3	0.2
18	18	19	0.0187	0.0133	0	0	Residential	0.12	0.08
19	19	20	0.0562	0.0397	64	39.5	Residential	0.18	0.12
20	20	21	0.0367	0.0247	64	39.5	Residential	0.18	0.12
21	21	22	0.0576	0.0308	0	0	Residential	0.18	0.12
22	22	23	0.0264	0.0192	64	39.5	Residential	0.12	0.08
23	23	24	0.0686	0.0499	0	0	Residential	0.24	0.16
24	24	25	0.0400	0.0283	0	0	Residential	0.18	0.12
25	25	26	0.0733	0.0533	127	79	Commercial	0.24	0.16
26	26	27	0.0337	0.0245	64	39.5	Residential	0.12	0.08
27	27	28	0.0587	0.0416	0	0	Residential	0.24	0.16
28	28	29	0.0658	0.0465	64	39.5	Residential	0.24	0.16
29	29	30	0.0344	0.0249	0	0	Residential	0.12	0.08
30	30	31	0.0129	0.0091	0	0	Residential	0.12	0.08

(*continued on next page*)

Table 11 (*continued*).

Branch number	Sending node	Receiving node	R (Ω)	X (Ω)	Active load (kW)	Reactive load (kvar)	Load type	λ_l	λ_d
31	31	32	0.0349	0.0246	127	79	Commercial	0.12	0.08
32	2	33	0.0445	0.0316	0	0	Residential	0.18	0.12
33	33	34	0.0020	0.0009	127	79	Commercial	0.06	0.04
34	5	35	0.2285	0.0557	255	158	Commercial	0.6	0.4
35	5	36	0.1271	0.1573	127	79	Commercial	0.36	0.24
36	6	37	0.0055	0.0073	42	26.3	Residential	0.06	0.04
37	37	38	0.2046	0.1447	0	0	Residential	0.6	0.4
38	38	39	0.0943	0.0666	17	10.5	Residential	0.3	0.2
39	39	40	0.0349	0.0246	0	0	Residential	0.12	0.08
40	40	41	0.0922	0.0653	64	39.5	Residential	0.3	0.2
41	41	42	0.2329	0.1648	0	0	Residential	0.6	0.4
42	42	43	0.1213	0.0858	0	0	Residential	0.36	0.24
43	43	44	0.0445	0.0316	42	26.3	Residential	0.18	0.12
44	44	45	0.0407	0.0289	0	0	Residential	0.18	0.12
45	45	46	0.0161	0.0128	0	0	Residential	0.12	0.08
46	46	47	0.0639	0.0452	0	0	Residential	0.24	0.16
47	47	48	0.0419	0.0296	106	65.8	Residential	0.18	0.12
48	48	49	0.0736	0.0512	127	79	Commercial	0.24	0.16
49	49	50	0.0832	0.0559	0	0	Residential	0.3	0.2
50	50	51	0.0400	0.0283	106	65.8	Residential	0.18	0.12
51	51	52	0.0226	0.0160	64	39.5	Residential	0.12	0.08
52	38	53	0.0845	0.0598	42	26.3	Residential	0.3	0.2
53	42	54	0.0162	0.0115	0	0	Residential	0.12	0.08
54	54	55	0.0530	0.0375	0	0	Residential	0.18	0.12
55	55	56	0.0897	0.0635	21	13.2	Residential	0.3	0.2
56	56	57	0.0871	0.0616	0	0	Residential	0.3	0.2
57	57	58	0.0677	0.0479	255	158	Commercial	0.24	0.16
58	58	59	0.0471	0.0334	127	79	Commercial	0.18	0.12
59	55	60	0.0336	0.0237	0	0	Residential	0.12	0.08
60	60	61	0.0329	0.0233	255	158	Commercial	0.12	0.08
61	61	62	0.0413	0.0292	170	105.4	Commercial	0.18	0.12
62	60	63	0.0355	0.0251	0	0	Residential	0.18	0.12
63	63	64	0.1052	0.0745	255	158	Commercial	0.36	0.24
64	64	65	0.0677	0.0479	127	79	Commercial	0.24	0.16
65	65	66	0.0303	0.0215	191	118.5	Commercial	0.12	0.08
66	66	67	0.0458	0.0325	42	26.3	Residential	0.18	0.12
67	67	68	0.0219	0.0155	85	52.7	Residential	0.12	0.08
68	63	69	0.0368	0.0260	255	158	Commercial	0.18	0.12
69	55	70	0.0232	0.0165	0	0	Residential	0.12	0.08
70	70	71	0.0121	0.0029	255	158	Commercial	0.12	0.08
71	70	72	0.0703	0.0497	127	79	Commercial	0.24	0.16
72	42	73	0.0232	0.0165	255	158	Commercial	0.12	0.08
73	73	74	0.0030	0.0064	255	158	Commercial	0.06	0.04
74	43	75	0.0381	0.0269	38	23.7	Residential	0.18	0.12
75	44	76	0.0555	0.0393	64	39.5	Residential	0.18	0.12
76	46	77	0.0518	0.0438	127	79	Commercial	0.18	0.12
77	76	78	0.0168	0.0111	0	0	Residential	0.12	0.08
78	78	79	0.0417	0.0101	427	264.7	Industrial	0.18	0.12
79	79	80	0.1008	0.0245	637	395.1	Industrial	0.3	0.2
80	79	81	0.1520	0.0372	0	0	Residential	0.48	0.32
81	81	82	0.0033	0.0008	127	79	Commercial	0.06	0.04
82	47	83	0.0085	0.0062	64	39.5	Residential	0.06	0.04
83	49	84	0.0519	0.0451	191	118.5	Commercial	0.18	0.12
84	50	85	0.0148	0.0036	0	0	Residential	0.12	0.08
85	85	86	0.0037	0.0016	425	263.4	Industrial	0.06	0.04
86	86	87	0.0000	0.0001	127	79	Commercial	0.06	0.04
87	7	88	0.0175	0.0232	64	39.5	Residential	0.12	0.08
88	88	89	0.0471	0.0628	55	34.2	Residential	0.18	0.12
89	89	90	0.0300	0.0400	0	0	Residential	0.12	0.08
90	90	91	0.0213	0.0284	0	0	Residential	0.12	0.08
91	91	92	0.0317	0.0422	0	0	Residential	0.12	0.08
92	92	93	0.0281	0.0375	0	0	Residential	0.12	0.08
93	93	94	0.0207	0.0275	93	57.9	Residential	0.12	0.08
94	94	95	0.0207	0.0275	0	0	Residential	0.12	0.08
95	89	96	0.0690	0.0488	127	79	Commercial	0.24	0.16
96	96	97	0.0975	0.0689	0	0	Residential	0.3	0.2
97	97	98	0.0906	0.0197	255	158	Commercial	0.3	0.2
98	97	99	0.0033	0.0008	0	0	Residential	0.06	0.04
99	99	100	0.0033	0.0008	255	158	Commercial	0.06	0.04
100	91	101	0.0232	0.0165	13	7.9	Residential	0.12	0.08
101	101	102	0.0581	0.0411	0	0	Residential	0.18	0.12
102	102	103	0.0893	0.0218	106	65.8	Residential	0.3	0.2

(*continued on next page*)

Table 11 (*continued*).

Branch number	Sending node	Receiving node	R (Ω)	X (Ω)	Active load (kW)	Reactive load (kvar)	Load type	λ_l	λ_d
103	103	104	0.0632	0.0154	0	0	Residential	0.24	0.16
104	104	105	0.1176	0.0286	255	158	Commercial	0.36	0.24
105	104	106	0.0115	0.0026	127	79	Commercial	0.06	0.04
106	92	107	0.0853	0.0208	427	264.7	Industrial	0.3	0.2
107	94	108	0.0615	0.0261	0	0	Residential	0.24	0.16
108	108	109	0.0454	0.0193	637	395.1	Industrial	0.18	0.12
109	94	110	0.0033	0.0008	637	395.1	Industrial	0.06	0.04
110	7	111	0.0722	0.0511	21	13.2	Residential	0.24	0.16
111	10	112	0.1075	0.0262	425	263.4	Industrial	0.36	0.24
112	11	113	0.0349	0.0246	64	39.5	Residential	0.12	0.08
113	13	114	0.0626	0.0443	0	0	Residential	0.24	0.16
114	114	115	0.0671	0.0475	0	0	Residential	0.24	0.16
115	115	116	0.0040	0.0010	255	158	Commercial	0.06	0.04
116	14	117	0.0508	0.0368	55	34.2	Residential	0.18	0.12
117	15	118	0.0162	0.0115	0	0	Residential	0.12	0.08
118	118	119	0.0464	0.0329	93	57.9	Residential	0.18	0.12
119	119	120	0.0426	0.0301	0	0	Residential	0.18	0.12
120	120	121	0.0509	0.0361	0	0	Residential	0.18	0.12
121	121	122	0.0736	0.0520	0	0	Residential	0.24	0.16
122	122	123	0.0587	0.0416	85	52.7	Residential	0.24	0.16
123	123	124	0.0613	0.0434	106	65.8	Residential	0.24	0.16
124	124	125	0.0787	0.0557	0	0	Residential	0.24	0.16
125	125	126	0.0838	0.0610	0	0	Residential	0.3	0.2
126	126	127	0.0349	0.0246	64	39.5	Residential	0.12	0.08
127	127	128	0.0573	0.0422	64	39.5	Residential	0.18	0.12
128	128	129	0.0588	0.0427	93	57.9	Residential	0.24	0.16
129	129	130	0.0103	0.0073	96	59.3	Residential	0.06	0.04
130	119	131	0.0357	0.0254	0	0	Residential	0.18	0.12
131	131	132	0.0349	0.0246	64	39.5	Residential	0.12	0.08
132	131	133	0.0924	0.0672	38	23.7	Residential	0.3	0.2
133	121	134	0.0845	0.0615	30	18.4	Residential	0.3	0.2
134	16	135	0.0530	0.0375	21	13.2	Residential	0.18	0.12
135	16	136	0.0303	0.0215	64	39.5	Residential	0.12	0.08
136	18	137	0.0587	0.0416	47	29	Residential	0.24	0.16
137	23	138	0.0773	0.0562	42	26.3	Residential	0.24	0.16
138	25	139	0.0955	0.0676	42	26.3	Residential	0.3	0.2
139	30	140	0.0522	0.0379	127	79	Commercial	0.18	0.12
140	31	141	0.0587	0.0416	64	39.5	Residential	0.24	0.16

References

[1] Jooshaki M, Karimi-Arpanahi S, Lehtonen M, Millar RJ, Fotuhi-Firuzabad M. An MILP model for optimal placement of sectionalizing switches and tie lines in distribution networks with complex topologies. IEEE Trans Smart Grid 2021.

[2] Jooshaki M, Karimi-Arpanahi S, Lehtonen M, Millar RJ, Fotuhi-Firuzabad M. Reliability-oriented electricity distribution system switch and tie line optimization. IEEE Access 2020;8:130967–78.

[3] Adefarati T, Bansal R. Reliability assessment of distribution system with the integration of renewable distributed generation. Appl Energy 2017;185:158–71.

[4] Lata P, Vadhera S. Reliability improvement of radial distribution system by optimal placement and sizing of energy storage system using TLBO. J Energy Storage 2020;30:101492.

[5] Ahmadi B, Ceylan O, Ozdemir A. Voltage profile improving and peak shaving using multi-type distributed generators and battery energy storage systems in distribution networks. In: 2020 55th international universities power engineering conference (UPEC). IEEE; 2020, p. 1–6.

[6] Kucevic D, Englberger S, Sharma A, Trivedi A, Tepe B, Schachler B, Hesse H, Srinivasan D, Jossen A. Reducing grid peak load through the coordinated control of battery energy storage systems located at electric vehicle charging parks. Appl Energy 2021;116936.

[7] Singh P, Meena NK, Yang J, Vega-Fuentes E, Bishnoi SK. Multi-criteria decision making monarch butterfly optimization for optimal distributed energy resources mix in distribution networks. Appl Energy 2020;278:115723.

[8] Das CK, Bass O, Mahmoud TS, Kothapalli G, Mousavi N, Habibi D, Masoum MA. Optimal allocation of distributed energy storage systems to improve performance and power quality of distribution networks. Appl Energy 2019;252:113468.

[9] Abniki H, Taghvaei SM, Mohammadi-Hosseininejad SM. Reliability improvement in smart grid through incorporating energy storage systems in service restoration. Int Trans Electr Energy Syst 2019;29(1):e2661.

[10] Ahmadi B, Ceylan O, Ozdemir A. Grey wolf optimizer for allocation and sizing of distributed renewable generation. In: 2019 54th international universities power engineering conference (UPEC). IEEE; 2019, p. 1–6.

[11] Ceylan O, Liu G, Tomsovic K. Coordinated distribution network control of tap changer transformers, capacitors and PV inverters. Electr Eng 2018;100(2):1133–46.

[12] Wolpert D, Macready W. No free lunch theorems for optimization. IEEE Trans Evol Comput 1997;1(1):67–82. http://dx.doi.org/10.1109/4235.585893.

[13] Naderipour A, Abdul Malek Z, Nowdeh SA, Ramachandaramurthy VK, Kalam A, Guerrero JM. Optimal allocation for combined heat and power system with respect to maximum allowable capacity for reduced losses and improved voltage profile and reliability of microgrids considering loading condition. Energy 2020;196:117124.

[14] Nikoobakht A, Aghaei J, Shafie-khah M, Catalao JPS. Allocation of fast-acting energy storage systems in transmission grids with high renewable generation. IEEE Trans Sustain Energy 2020;11(3):1728–38.

[15] De la Nieta AAS, Ilieva I, Gibescu M, Bremdal B, Simonsen S, Gramme E. Optimal midterm peak shaving cost in an electricity management system using behind customers' smart meter configuration. Appl Energy 2021;283:116282.

[16] Uddin M, Romlie M, Abdullah M, Tan C, Shafiullah G, Bakar AHA. A novel peak shaving algorithm for islanded microgrid using battery energy storage system. Energy 2020;196:117084.

[17] Maeyaert L, Vandevelde L, Döring T. Battery storage for ancillary services in smart distribution grids. J Energy Storage 2020;30:101524.

[18] Hamidan M-A, Borousan F. Optimal planning of distributed generation and battery energy storage systems simultaneously in distribution networks for loss reduction and reliability improvement. J Energy Storage 2022;46:103844.

[19] Alam A, Pant V, Das B. Optimal placement of protective devices and switches in a radial distribution system with distributed generation. IET Gener Trans Distrib 2020;14(21):4847–58.

[20] Alam A, Alam MN, Pant V, Das B. Placement of protective devices in distribution system considering uncertainties in loads, temporary and permanent failure rates and repair rates. IET Gener Trans Distrib 2017;12(7):1474–85.

[21] Marqusee J, Becker W, Ericson S. Resilience and economics of microgrids with PV, battery storage, and networked diesel generators. Adv Appl Energy 2021;100049.

[22] Amohadi M, Fotuhi-Firuzabad M. Optimal placement of automatic switching equipment in radial distribution networks based on protective coordination. J Electr Eng Technol 2019;14(3):1127–37.

[23] Moradi A, Fotuhi-Firuzabad M. Optimal switch placement in distribution systems using trinary particle swarm optimization algorithm. IEEE Trans Power Deliv 2007;23(1):271–9.

[24] Rodrigues FM, de Araujo LR, Penido DRR. Improvement of reliability indices and costs in distribution systems considering multiple scenarios through switch reallocation. J Control, Autom Electr Syst 2020;31(6):1508–19.

[25] Nikkhah S, Rabiee A, et al. Multi-objective stochastic model for joint optimal allocation of DG units and network reconfiguration from DG owner's and disco's perspectives. Renew Energy 2019;132:471–85.
[26] Hamida IB, Salah SB, Msahli F, Mimouni MF. Optimal network reconfiguration and renewable DG integration considering time sequence variation in load and DGs. Renew Energy 2018;121:66–80.
[27] Jangdoost A, Keypour R, Golmohamadi H. Optimization of distribution network reconfiguration by a novel RCA integrated with genetic algorithm. Energy Syst 2020;1–33.
[28] Abbasi AR, Seifi AR. Considering cost and reliability in electrical and thermal distribution networks reinforcement planning. Energy 2015;84:25–35.
[29] Wang J, Yang W, Du P, Niu T. A novel hybrid forecasting system of wind speed based on a newly developed multi-objective sine cosine algorithm. Energy Convers Manage 2018;163:134–50.
[30] Mirjalili S, Saremi S, Mirjalili SM, Coelho LdS. Multi-objective grey wolf optimizer: a novel algorithm for multi-criterion optimization. Expert Syst Appl 2016;47:106–19.
[31] Premkumar M, Jangir P, Sowmya R, Alhelou HH, Heidari AA, Chen H. MOSMA: Multi-objective slime mould algorithm based on elitist non-dominated sorting. IEEE Access 2020;9:3229–48.
[32] Srinivas N, Deb K. Muiltiobjective optimization using nondominated sorting in genetic algorithms. Evol Comput 1994;2(3):221–48.
[33] Mongird K, Viswanathan VV, Balducci PJ, Alam MJE, Fotedar V, Koritarov VS, Hadjerioua B. Energy storage technology and cost characterization report. Technical Report, Pacific Northwest National Lab.(PNNL), Richland, WA (United States); 2019.
[34] Fu R, Feldman DJ, Margolis RM. US solar photovoltaic system cost benchmark: Q1 2018. Technical Report, National Renewable Energy Lab.(NREL), Golden, CO (United States); 2018.
[35] Wiser R, Bolinger M. 2018 Wind technologies market report. 2020, URL: https://www.energy.gov/eere/wind/downloads/2018-wind-technologies-market-report, (accessed June 6, 2020).
[36] Allan RN, et al. Reliability evaluation of power systems. Springer Science & Business Media; 2013.
[37] Tawhid MA, Savsani V. Multi-objective sine-cosine algorithm (MO-SCA) for multi-objective engineering design problems. Neural Comput Appl 2019;31(2):915–29.
[38] Mirjalili S. SCA: a sine cosine algorithm for solving optimization problems. Knowl-Based Syst 2016;96:120–33.
[39] Ahmadi B, Ceylan O, Ozdemir A. A multi-objective optimization evaluation framework for integration of distributed energy resources. J Energy Storage 2021;41:103005.
[40] Eminoglu U, Hocaoglu MH. Distribution systems forward/backward sweep-based power flow algorithms: a review and comparison study. Electr Power Compon Syst 2008;37(1):91–110.
[41] Baran ME, Wu FF. Network reconfiguration in distribution systems for loss reduction and load balancing. IEEE Trans Power Deliv 1989;4:1401–7.
[42] Das D. Optimal placement of capacitors in radial distribution system using a Fuzzy-GA method. Int J Electr Power Energy Syst 2008;30(6–7):361–7.
[43] Khodr H, Olsina F, Jesus PDO-D, Yusta J. Maximum savings approach for location and sizing of capacitors in distribution systems. Electr Power Syst Res 2008;78:1192–203.
[44] Ahmadi B, Younesi S, Ceylan O, Ozdemir A. Multi-objective distributed energy resource integration in radial distribution networks. In: 56th international universities power engineering conference (UPEC). IEEE; 2021, p. 1–6.
[45] Ahmadi B, Younesi S, Ceylan O, Ozdemir A. The arithmetic optimization algorithm for optimal energy resource planning. In: 56th international universities power engineering conference (UPEC). IEEE; 2021, p. 1–6.
[46] Staffell I, Pfenninger S. Using bias-corrected reanalysis to simulate current and future wind power output. Energy 2016;114:1224–39.
[47] Pfenninger S, Staffell I. Long-term patterns of European PV output using 30 years of validated hourly reanalysis and satellite data. Energy 2016;114:1251–65.
[48] Atwa YM, El-Saadany E. Optimal allocation of ESS in distribution systems with a high penetration of wind energy. IEEE Trans Power Syst 2010;25(4):1815–22.
[49] Zitzler E, Thiele L. Multiobjective optimization using evolutionary algorithms—a comparative case study. In: International conference on parallel problem solving from nature. Springer; 1998, p. 292–301.
[50] Wang B, Singh HK, Ray T. Adjusting normalization bounds to improve hypervolume based search for expensive multi-objective optimization. Complex Intell Syst 2021;1–17.
[51] Santiago A, Dorronsoro B, Fraire HJ, Ruiz P. Micro-genetic algorithm with fuzzy selection of operators for multi-objective optimization: μFAME. Swarm Evol Comput 2021;61:100818.
[52] Fleischer M. The measure of Pareto optima applications to multi-objective metaheuristics. In: International conference on evolutionary multi-criterion optimization. Springer; 2003, p. 519–33.

Bahman Ahmadi

Oguzhan Ceylan

Aydogan Ozdemir

Mahmoud Fotuhi-Firuzabad